2019 19th International Conference on Control, Automation and Systems (ICCAS 2019)
Oct. 15~18, 2019; ICC Jeju, Jeju, Korea

Development of Confidence Bound Visualization Tool for LTE-Based UAV Surveillance in Urban Areas

Halim Lee[1,2], Taewon Kang[1,2], and Jiwon Seo[1,2*]

[1] School of Integrated Technology, Yonsei University,
Incheon, 21983, Korea (halim.lee, taewon.kang, jiwon.seo@yonsei.ac.kr)
[2] Yonsei Institute of Convergence Technology, Yonsei University,
Incheon, 21983, Korea
* Corresponding author

Abstract: We have developed a tool to visualize a situation of estimating the positions of unmanned aerial vehicles (UAVs) using long-term evolution (LTE) signals in an urban area. In our visualization tool, true positions of UAVs and evolved Node Bs (eNodeBs), estimated positions of UAVs, and the calculated horizontal and vertical protection levels (HPLs and VPLs) are displayed in a 3D city map. For a realistic simulation, the 3D city map is generated using real buildings and terrain data of Gangnam, Seoul, Korea. Users can directly specify the locations of UAVs and eNodeBs to simulate these cases. Error variances are added to the true range between UAVs and eNodeBs in the developed tool. Next, the position and the HPL and VPL of each UAV are calculated and displayed on the map. Using the developed visualization tool, we observed changes in the estimated positions and confidence bounds of UAVs by adjusting the number of eNodeBs transmitting LTE signals. Simulation results show that the size of confidence bounds decreases as the number of eNodeBs increases.

Keywords: LTE, integrity, protection level, urban area, UAV

1. INTRODUCTION

Recently, as demand for unmanned aerial vehicles (UAVs) has increased in the private industries [1, 2], the need for unmanned aircraft system traffic management (UTM) has emerged [3]. UTM is a system that manages the flight paths and operations of small UAVs within 150 m of ground in low-altitude airspace [4]. In a UTM system, the development of a reliable navigation technology is actively studied to support safe and efficient operation of UAVs [5–8]. The navigation technology can be used in situations such as collision avoidance [9] and electronic toll collection (ETC) [10].

As an example of a navigation system, the global navigation satellite systems (GNSSs) such as the Global Positioning System (GPS) provide accurate position and timing information [11–17]. However, in some challenging areas, because of the weak signals of GNSS and environmental problems, it is necessary to develop other navigation systems that assist GNSS. Accordingly, alternative navigation technologies such as long-range navigation (Loran) were studied for maritime navigation [18, 19].

For use in urban areas, navigation system using cellular signals has advantages of high signal strength and geometric diversity [20]. Consequently, many studies using long-term evolution (LTE) downlink signals have begun to emerge [21–23]. In recent studies, the positioning accuracy using LTE signals was reported at the meter level [24, 25].

In this study, we developed a visualization tool to display the horizontal confidence bounds, also known as horizontal protection levels (HPLs), of LTE-based positioning solutions for the surveillance of UAVs in a realistic 3D city map to support the management of the traffic of UAVs in urban areas. Furthermore, we displayed the vertical protection levels (VPLs) derived from the pseudorange error variances of both barometric altimeter [26] and LTE signals [23, 24]. In our tool, we created a map of an actual urban area, Gangnam, Seoul, Korea. Users can place the Evolved Node Bs (eNodeBs) and UAVs on the map and simulate the various deployments. As a result of the simulation, the true and estimated positions, HPLs, and VPLs of UAVs are visualized on the map. In this paper, we conducted a simulation while adjusting the number of eNodeBs.

This paper is organized as follows: Section 2 introduces the calculation method of the HPL and VPL. Section 3 describes the settings, such as map generation and placement of eNodeBs and UAVs, for simulation. Section 4 shows the simulation results achieved by changing the number of eNodeBs. Finally, in Section 5, we concluded the paper.

2. PL CALCULATION METHOD

The VPL and HPL are computed using methods described in [27, appendix J]. In addition, we utilized the method used in [26] for the addition of external altitude measurements from barometric altimeter. It is assumed that LTE signals are used to calculate the HPL, and both LTE signals and barometric altimeter are used to calculate the VPL.

In fault-free case, the HPL and VPL can be derived from two steps [28]: converting pseudorange domain variance to position domain variance, and scaling position variance as per the integrity requirement.

2.1 Conversion to position domain variance

We assumed the pseudorange error from the i th eNodeB or barometric altimeter as zero mean, normal

distribution. The position error variance for each direction can then be expressed as follows. (The equations in this subsection are adapted from [27, appendix J]. We modified the equations in [27] to consider a barometric altimeter measurement according to [26].)

$$\text{East: } d_{east}^2 = \sum_{i=1}^{N} s_{east,i}^2 \sigma_i^2, \quad (1)$$

$$\text{North : } d_{north}^2 = \sum_{i=1}^{N} s_{north,i}^2 \sigma_i^2, \quad (2)$$

$$\text{Vertical: } d_v^2 = \sum_{i=1}^{N} s_{v,i}^2 \sigma_i^2, \quad (3)$$

, where, σ_i^2 is the pseudorange error variance from the ith eNodeB or barometric altimeter. d_{east}, d_{north}, and d_v are the error uncertainty for the east, north, and vertical axis, respectively.

The vector s is defined as a unit vector from the user towards the ith eNodeB or barometric altimeter. The $s_{east,i}$, $s_{north,i}$, and $s_{v,i}$ refer to the partial derivative of position error along the east, north, and vertical direction, respectively. The vector s is also an element of the projection matrix S that is derived using the weighted least-squares method.

$$S = \begin{bmatrix} s_{east,1} & \cdots & s_{east,N} \\ s_{north,1} & \ddots & s_{north,N} \\ s_{v,1} & & s_{v,N} \\ s_{t,1} & \cdots & s_{t,N} \end{bmatrix} = (G_{LTE+Alt}^T \cdot W \cdot G_{LTE+Alt})^{-1} \cdot G_{LTE+Alt}^T \cdot W, \quad (1)$$

, where the ith row of the geometry matrix G_{LTE} is defined in Eq. (5), when positive azimuth is defined clockwise from North. The subscript LTE means that only LTE signals are used. In Eq. (6), we modified the geometry matrix to $G_{LTE+Alt}$ to include external altitude measurement, assuming that the barometric altimeter is available. Also, a diagonal matrix of weights W is defined in Eq. (7). In Eq. (7), σ_{Alt}^2 means pseudorange error variance of barometric altimeter.

$$G_i = \begin{bmatrix} -\cos El_i \sin Az_i & -\cos El_i Az_i & -\sin El_i & 1 \end{bmatrix}, \quad (5)$$

$$G_{LTE+Alt} = \begin{bmatrix} G_{LTE} \\ 0 \quad 0 \quad 1 \quad 0 \end{bmatrix}, \quad (6)$$

$$W^{-1} = \begin{bmatrix} \sigma_1^2 & 0 & \cdots & 0 \\ 0 & \sigma_2^2 & & \vdots \\ \vdots & & \ddots & 0 \\ 0 & \ldots & 0 & \sigma_{Alt}^2 \end{bmatrix}, \quad (7)$$

2.2 Scaling to integrity requirement

The probability of missed detection of a misleading information (MI) event is defined as β. Next, we obtained a factor K corresponding to the probability β from the standard normal distribution. The formula for obtaining K_H and K_V are expressed in Eqs. (8) and (9) [27].

$$K_H = \Phi^{-1}(1 - \beta_H/2), \quad (8)$$

$$K_V = \Phi^{-1}(1 - \beta_V/2), \quad (9)$$

In Eqs. (8) and (9), Φ denotes the cumulative distribution function (CDF) of the standard normal distribution. The subscript H and V refer to horizontal and vertical, respectively.

As a result, we obtained HPL and VPL using following equations:

$$HPL = K_H d_{major}, \quad (10)$$

$$VPL = K_v d_v, \quad (11)$$

, where d_{major} is the error uncertainty for the semi-major axis of an ellipse, which is expressed in Eq. (12) [27]. In Eq. (13), d_{EN} is covariance of error distribution in the east and north axis.

$$d_{major}{}^2 = \frac{d_{east}^2 + d_{north}^2}{2} + \sqrt{\left(\frac{d_{east}^2 - d_{north}^2}{2}\right)^2 + d_{EN}^2}, \quad (12)$$

$$d_{EN}^2 = \sum_{i=1}^{N} s_{east,i} s_{north,i} \sigma_i^2, \quad (13)$$

3. SIMULATION SETTINGS

We generated the 3D map of an urban area in Gangnam, Seoul, Korea using the method proposed in [29]. We used a 3D elevation model and building data from the VWorld's open application programming interface (API) [30].

We decided the location of the eNodeBs and UAVs on the East-North-Up (ENU) coordinate system based on the center of the intersection of Gangnam Station. The ENU coordinates of each eNodeB and UAV selected for the simulations are shown in Tables 1 and 2, respectively. Furthermore, Fig. 1 shows the positions of eNodeBs and UAVs on the map.

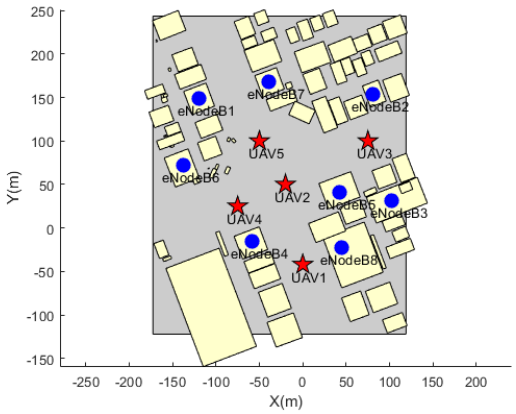

Fig. 1 Positions of eNodeBs (blue circles) and UAVs (red stars) on map

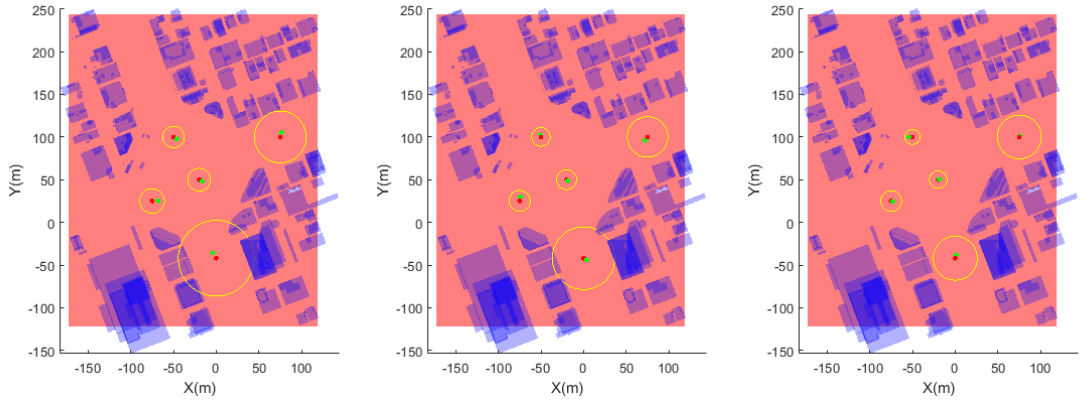

Fig. 2 Top view of simulation results with eNodeB numbers ranging from 1 to 4 (left), 1 to 6 (middle), and 1 to 8 (right). Red and green dots indicate the true position and estimated positions of UAVs, respectively. Yellow cylinder indicates confidence bound of each UAV position, for which the radius is HPL and half of the height is VPL.

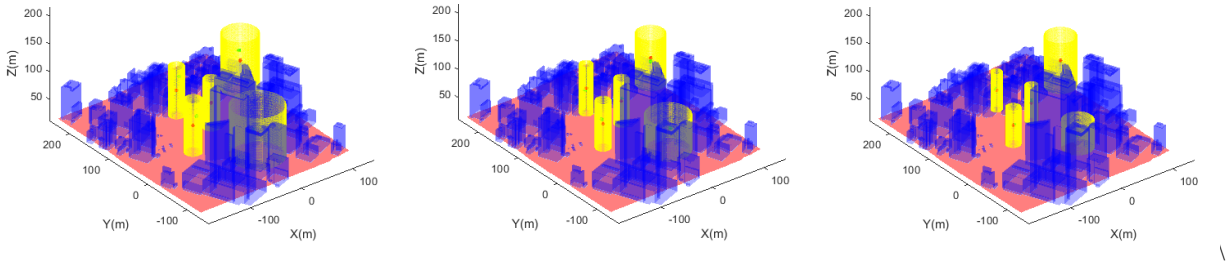

Fig. 3 Side view of simulation results with eNodeB numbers ranging from 1 to 4 (left), 1 to 6 (middle), and 1 to 8 (right). Red and green dots indicate the true position and estimated positions of UAVs, respectively. Yellow cylinder indicates confidence bound of each UAV position, for which the radius is HPL and half of the height is VPL.

Table 1 ENU coordinates of eNodeBs (unit: **m**)

eNodeB Number	x	y	z
1	−119.55	148.92	78.57
2	80.70	153.72	64.21
3	102.29	31.41	30.23
4	−58.40	−15.36	92.25
5	42.33	41.00	118.47
6	−137.54	72.18	91.73
7	−39.21	168.11	102.51
8	44.73	−22.55	160.39

Table 2 ENU coordinates of UAVs (unit: **m**)

UAV Index	x	y	z
1	0	−42	60
2	−20	50	80
3	75	100	100
4	−75	25	70
5	−50	100	90

Standard deviation of pseudorange error from LTE signals are assumed as $\sigma_{LTE} = 2.8959$ (m). This value is the average variance of LTE pseudorange errors in the literature (Table 4 of [24]). In addition, we determined pseudorange error variance from barometric altimeter $\sigma_{Alt} = 11.7275$ (m) with reference to [26]. We also set both β_V and β_H values to 10^{-5} in the simulation. The estimated positions of the UAVs were calculated using the recursive least-squares (RLS) algorithm that is introduced in [31].

4. SIMULATION RESULTS

Figs. 2 and 3 show the example of HPL and VPL calculation results and the estimated positions of each UAV from top and side view, respectively. The results of adjusting eNodeB numbers from 1 to 4, 1 to 6, and 1 to 8 were displayed. For yellow cylinders, the radius is HPL and half of the height is VPL. In addition, green and red dots represent the estimated position and true position of UAVs, respectively.

Tables 3 and 4 show the values of HPLs and VPLs of UAVs depending on the number of eNodeBs, respectively. The PLs in Tables 3 and 4 are obtained by averaging the PLs from 100 simulation runs. The mean values of HPLs are 23.00 m, 19.83 m, and 16.89 m with eNodeB numbers ranging from 1 to 4, 1 to 6, and 1

to 8, respectively. Also, the mean values of VPLs are 47.50 m , 39.32 m , and 33.60 m with eNodeB numbers ranging from 1 to 4, 1 to 6, and 1 to 8, respectively. As expected, the simulation results show that the size of the HPL and VPL tends to decrease as the number of eNodeBs increases.

Table 3 HPLs of UAVs depending on the number of eNodeBs (unit: **m**)

		eNodeB Number		
		1 to 4	**1 to 6**	**1 to 8**
UAV Index	**1**	43.48	35.90	27.61
	2	13.64	11.92	10.25
	3	26.43	25.35	25.15
	4	18.96	14.68	12.36
	5	12.47	11.31	9.10
Mean		23.00	19.83	16.89

Table 4 VPLs of UAVs depending on the number of eNodeBs (unit: **m**)

		eNodeB Number		
		1 to 4	**1 to 6**	**1 to 8**
UAV Index	**1**	48.45	29.28	25.58
	2	46.81	38.24	30.75
	3	47.78	45.69	43.99
	4	49.07	40.88	32.86
	5	45.37	42.49	34.81
Mean		47.50	39.32	33.60

5. CONCLUSION

We have developed a visualization tool for LTE-based surveillance of UAVs in an urban area. User can select the number and position of UAVs and eNodeBs in the developed tool. We have calculated the estimated positions, HPLs, and VPLs of UAVs, and plotted them on an actual urban map. In addition, we have shown through simulation that the PL size tends to decrease as the number of eNodeBs increases as expected.

ACKNOWLEDGMENTS

This research was supported by a grant (18CTAP-C143427-01) from the Technology Advancement Research Program funded by the Ministry of Land, Infrastructure and Transport of the Korean government. Also, this research was supported by the Ministry of Science and ICT (MSIT), Korea, under the "ICT Consilience Creative Program" (IITP-2019-2017-0-01015) supervised by the Institute of Information & Communications Technology Planning & Evaluation (IITP).

REFERENCES

[1] F. Kendoul, "Survey of advances in guidance, navigation, and control of unmanned rotorcraft systems," *Journal of Field Robotics*, Vol. 29, No. 2, pp. 315-378, 2012.

[2] K. Nonami, F. Kendoul, S. Suzuki, W. Wang, and D. Nakazawa, "Autonomous flying robots: unmanned aerial vehicles and micro aerial vehicles," *Springer Science & Business Media*, 2010.

[3] A. Puri, "A survey of unmanned aerial vehicles (UAV) for traffic surveillance," *Department of Computer Science and Engineering, University of South Florida*, pp. 1-29, 2005.

[4] P. Kopardekar, J. Rios, T. Prevot, M. Johnson, J. Jung, and J. E. Robinson, "Unmanned aircraft system traffic management (UTM) concept of operations," *16th AIAA Aviation, Technology, Integration, and Operations Conference*, 2016.

[5] A. Rucco, P. B. Sujit, A. P. Aguiar, J. B. De Sousa, and F. L. Pereira, "Optimal rendezvous trajectory for unmanned aerial-ground vehicles," *IEEE Transactions on Aerospace and Electronic Systems*, Vol. 54, No. 2, pp. 834-847, 2018.

[6] J. H. Kim, J.-W. Kwon, and J. Seo, "Multi-UAV-based stereo vision system without GPS for ground obstacle mapping to assist path planning of UGV," *Electronics Letters*, Vol. 50, No. 20, pp. 1431-1432, 2014.

[7] Y. H. Shin, S. Lee, and J. Seo, "Autonomous safe landing-area determination for rotorcraft UAVs using multiple IR-UWB radars," *Aerospace Science and Technology*, Vol. 69, pp. 617-624, 2017.

[8] H. Lee, W. Kim, and J. Seo, "Simulation of UWB radar-based positioning performance for a UAV in an urban area," *2018 IEEE International Conference on Consumer Electronics-Asia (ICCE-Asia)*, pp. 206-212, 2018.

[9] Y. K. Kwag and C. H. Chung, "UAV based collision avoidance radar sensor," *2007 IEEE International Geoscience and Remote Sensing Symposium*, 2007.

[10] D. Salós, A. Martineau, C. Macabiau, B. Bonhoure, and D. Kubrak, "Receiver autonomous integrity monitoring of GNSS signals for electronic toll collection," *IEEE Transactions on Intelligent Transportation Systems*, Vol. 15, No. 1, pp. 94-103, 2013.

[11] P. Misra and P. Enge, *Global Positioning System: Signals, Measurements, and Performance*, Ganga-Jamuna Press, Lincoln, MA, USA, 2011.

[12] J. Lee, Y. T. Morton, J. Lee, H.-S. Moon, and J. Seo, "Monitoring and mitigation of ionospheric anomalies for GNSS-based safety critical systems," *IEEE Signal Processing Magazine*, Vol. 34, No. 5, pp. 96-110, 2017.

[13] D. Yoon, C. Kee, J. Seo, and B. Park, "Position accuracy improvement by implementing the DGNSS-CP algorithm in smartphones," *Sensors*,

Vol. 16, No. 6, Art. No. 910, 2016.
[14] D. S. De Lorenzo, S. C. Lo, J. Seo, Y.-H. Chen, and P. K. Enge, "The WAAS/L5 signal for robust time transfer: Adaptive beamsteering antennas for satellite time synchronization," *Proc. of the ION GNSS 2010*, pp. 2106-2116, 2010.
[15] J. Seo and T. Walter, "Future dual-frequency GPS navigation system for intelligent air transportation under strong ionospheric scintillation," *IEEE Transactions on Intelligent Transportation Systems*, Vol. 15, No. 5, pp. 2224-2236, 2014.
[16] K. Park, D. Lee, and J. Seo, "Dual-polarized GPS antenna array algorithm to adaptively mitigate a large number of interference signals," *Aerospace Science and Technology*, Vol. 78, pp. 387-396, 2018.
[17] M. Kim, J. Seo, and J. Lee, "A comprehensive method for GNSS data quality determination to improve ionospheric data analysis," *Sensors*, Vol. 14, No. 8, pp. 14971-14993, 2014.
[18] S. C. Lo, B. B. Peterson, T. Hardy, and P. K. Enge, "Improving Loran coverage with low power transmitters," *Journal of Navigation*, Vol. 63, No. 1, pp. 23-38, 2010.
[19] P.-W. Son, J. H. Rhee, and J. Seo, "Novel multichain-based Loran positioning algorithm for resilient navigation," *IEEE Transactions on Aerospace and Electronic Systems*, Vol. 54, No. 2, pp. 666-679, 2018.
[20] Z. Z. M. Kassas, J. Khalife, K. Shamaei, and J. Morales, "I hear, therefore I know where I am: Compensating for GNSS limitations with cellular signals," *IEEE Signal Processing Magazine*, Vol. 34, No. 5, pp. 111-124, 2017.
[21] J. A. del Peral-Rosado, J. A. López-Salcedo, G. Seco-Granados, F. Zanier, P. Crosta, R. loannides, and M. Crisci, "Software-defined radio LTE positioning receiver towards future hybrid localization systems," *31st AIAA International Communications Satellite Systems Conference*, 2013.
[22] M. Driusso, C. Marshall, M. Sabathy, F. Knutti, H. Mathis, and F. Babich, "Vehicular position tracking using LTE signals," *IEEE Transactions on Vehicular Technology*, Vol. 66, No. 4, pp. 3376-3391, 2017.
[23] K. Shamaei, J. Khalife, and Z. M. Kassas, "Exploiting LTE signals for navigation: Theory to implementation," *IEEE Transactions on Wireless Communications*, Vol. 17, No. 4, pp. 2173-2189, 2018.
[24] K. Shamaei and Z. M. Kassas, "LTE receiver design and multipath analysis for navigation in urban environments," *Navigation*, Vol. 65, No. 4, pp. 655-675, 2018.
[25] M. Maaref, J. Khalife, and Z. M. Kassas, "Integrity Monitoring of LTE Signals of Opportunity-Based Navigation for Autonomous Ground Vehicles," *Proc. of the ION GNSS 2018*, pp. 2456-2466, 2018.
[26] S. S. Jan, D. Gebre-Egziabher, T. Walter, and P. Enge, "Improving GPS-based landing system performance using an empirical barometric altimeter confidence bound," *IEEE Transactions on Aerospace and Electronic Systems*, Vol. 44, No. 1, pp. 127-146, 2008.
[27] SC, RTCA, "Minimum Operational Performance Standards for Global Positioning System/Wide Area Augmentation System Airborne Equipment," *RTCA/DO-229C*, 2001.
[28] B. Roturier, E. Chatre, J. Ventura-Traveset, "The SBAS integrity concept standardised by ICAO-application to EGNOS," *Navigation (Paris)*, Vol. 49, pp. 65-77, 2001.
[29] W. Kim, T. Kang, and J. Seo, "Software-based model of urban canyon effect on GPS signals using 3D map data," *Proc. of the IRES - 79th International Conference on Science, Technology and Management*, Vienna, Austria, Art. No. 2656, 2016.
[30] VWorld Open API, Available: http://dev.vworld.kr
[31] A. Norrdine, "An algebraic solution to the multilateration problem," *Proc. of the 15th International Conference on Indoor Positioning and Indoor Navigation*, Sydney, Australia, Vol. 1315, 2012.